Global Scientific JOURNALS

GSJ: Volume 10, Issue 9, September 2022, Online: ISSN 2320-9186

www.globalscientificjournal.com

SYNTHESIS AND CONJUGATION OF SILVER NANOPARTICLES WITH BETA AMPICILLIN (2) ANTIBIOTIC

Onyangore, H. D. M1*. Andala, D.1, and Ndangili, P.2

Department of Chemistry, The Multimedia University of Kenya, Nairobi, Kenya. P.O. Box 15653- 00503 Nairobi, Kenya

School of Chemistry and Material Science, The Technical University of Kenya, Nairobi, Kenya. P.O. Box 52428 - 00200. Nairobi- Kenya

*Corresponding author: E-mail: honyangore@gmail.com Cell:

+254-724-685-368

Abstract

This paper sets out to determine whether silver nanoparticles conjugation enhance the antibacterial efficacy of clinically approved drugs. Antimicrobial resistance (AMR) arises when microorganisms undergo gene mutation upon exposure to antimicrobial drugs. The increase of drug resistance among pathogenic bacteria has augmented the search for new antimicrobials or modifying those available to boost antibacterial activity. The most promising and novel antimicrobial agents are metal nanoparticles. Before the discovery of antibiotics, silver nitrate and silver sulfadiazine were used to treat skin infections. The main aim of this research was to synthesize, characterize, and carry out *in vitro* assay for silver nanoparticles (Ag-NPs) conjugated to ampicillin (2). Ag-NPs were synthesized chemically using sodium citrate whereby the pristine Ag-NPs had a dark grey colour and their formation was checked via UV-VIS spectrophotometer. They exhibited a characteristic Surface Plasmon Resonance (SPR) band at 421 nm with smaller particle size and shifted blue, confirming Ag-NPs synthesis. Fourier transform infrared (FT- IR) spectroscopic methods exhibited various functional groups within the range of 4000–400 cm^{-1}. Cyclic voltammetry confirmed the conjugation of antibiotics to Ag metal. The voltammetry of pure unconjugated antibiotic (2), and their conjugates showed Newtonian behaviour. The Dynamic light scattering (DLS) size distribution ranged from 41 nm to 44 nm, Polydispersity Index (PDI) ranged from 0.511 to 0.589, and zeta potential, ranged from -9.16 to -15.2 for Ag-NPs. Ag- NPs/antibiotic conjugates size distribution ranged from 120 nm to 395 nm, PDI ranged from 0.256 to 0.440, and zeta potential ranged from -11.2 to -35.9. *In vitro* bioassays of conjugated ampicillin (2) exemplified a significant difference ($p<0.01$) and exhibited effective synergistic effects against *E. coli* and

S. aureus against ampicillin (2) alone.

Keywords: Ampicillin (2), cyclic voltammetry, nanoparticles, antibacterial, nanotechnology

1. Introduction

Infectious diseases are a significant burden on public health, driven largely by socio-economic, environmental and ecological factors. About 15 million of 57 million annual deaths worldwide are estimated to be caused by infectious diseases, principally due to bacterial pathogens. The burden of morbidity and mortality falls most heavily on people in developing countries Bulk silver historically has been used as an antimicrobial [1]. Metal particles (NPs) of ultrafine size have attracted abundant attention because of their unusual properties distinguishable from those of their bulk equivalents [2]. NPs are tiny materials having size ranges from 1 to 100 nm. Both chemical and physical properties of the metal NPs are reliant on their size, structure &shape and size distribution[3]. Thus it is crucial to control size and size distribution by varying the synthesis methods, reducing agents and stabilizers[4-6]. The physical methods, metallic NPs prepared through laser ablation [7], evaporation/condensation[8], and UV irradiation [9] and produce particles in nano sizes. However abundant reports on chemical methods can be found only in the literature. Chemical reduction due to its simplicity is widely used and also allows variation in the molar concentration of the reactant, dispersant and feed rate of reactant in order to produce silver nanoparticles with controlled particle sizes, shapes and particle size distribution [8]. The selection of an appropriate reducing agent is also a crucial factor, as the size, shape and particle size distribution strongly depend on the nature of the reducing agent [8]. When the reducing agent is introduced it causes the reduction of metal precursor [10]. Reduction of metal salts requires adjustment of the reactivity of the reducing agent to the redox potential of the metal[8, 10]. During the synthesis process, if the reaction rate is too fast, rapid formation of a large amount of metal nuclei will occur and result in particles that are too small[4, 8-10]. Surface functionalization is the conjugation of Ag-NPs with bioactive molecules to produce entirely new functions. Ag-NPs surface has a high affinity for sulfhydryl (thiol) groups. These strong ligand-interface interactions control NP growth and become a unique modulation strategy for creating unconventional plasmonic hybrid nanostructures[11]. [12] reported the adsorption of ampicillin (2) on citrate coated chemically synthesized silver and gold nanoparticles. They suggested in their study that the antibiotic attaches to silver/gold nanoparticles via thioether moiety. [13], compared the binding/adsorption of ampicillin (2) to chemically synthesized nanoparticles coated with sodium citrate and biologically synthesized nanoparticles. Their observation was that adsorption of ampicillin on citrate capped silver

nanoparticles is less stable compared to biological synthesis may be due to disequilibrium in binding of silver to the negatively charged citrate. The bio conjugation ampicillin adsorption nanoparticles, is more stable due to coating with an organic layer, acting as a stabilizer.

There an urgent need to advance novel and efficient procedures to conjugate silver nanoparticles with beta lactam based penicillin drugs. There are very few reports available for silver nanoparticle conjugation using beta lactam based drugs and trisodium citrate as a stabilizer, but also so far no reports on characterization of these conjugates using cyclic voltammetry. Therefore, in the present work silver nanoparticles and ampicillin (2) (a beta lactam antibiotic), were chemically synthesized and subjected to In vitro assay using *E. coli* and *S. aureus.*

1.1. Materials

1.1.1 Chemicals, Reagents, and Solvents

All materials were of analytical grade; they were used without further purification. Deionized water (DW) which was obtained with a Werkstoff polyethylen DI generator from Thermo Fisher Scientific (Kenya). All of the media were purchased from Oxoid limited, Basingstoke, United Kingdom. Analytical grade Silver nitrate ($AgNO_3$) and Sodium citrate ($Na_3C_6H_5O_7$) were purchased from *Sigma-Aldrich,* represented in Kenya by Kobian Scientific.

1.1.2 Instruments

UV-VIS spectrophotometer (Shimadzu UV-1850), FT-IR spectrophotometer (Thermo Scientific Instruments, USA. To obtain a good signal to noise ratio, 32 scans of antibiotic (2), purified Ag-NPs and their antibiotic conjugates were taken in the range 4000–400 cm^{-1} and the resolution was kept at 4.0 cm^{-1}[14, 15]. Dynamic light scattering (DLS) measurements were carried out using the Zetasizer Nano ZS (Malvern Panalytical Scientific, USA). 2450-EC system for cyclic voltammetry (CV), in vitro assay was performed by Agar cup diffusion.

1.1.3 Laboratory Procedure

1.1.3.1 Silver nanoparticles Synthesis/ Characterization

The synthesis of Ag-NPs using the chemical reduction method[8]. 90mg $AgNO_3$ and 500 mL deionized water (DW) dissolved 90 mg in a 500ml Erlenmeyer flask, boiled on a hot plate stirrer Labtech (Daihan Labtech Co. Ltd). Ag-NPs were obtained with a dropwise injection rate of 10mL aliquot of 1% trisodium citrate solution to the boiling solution with vigorous stirring and a reaction temperature of 100 °C. The resulting solution was continuously boiled for further 10 minutes until a grey dispersion appeared. A blank analysis was carried out using the same procedure excluding $AgNO_3$ with no colour change.The grey dispersion was separated by centrifugation at 2000 RPM for 10 minutes. Trisodium citrate was used both as a capping and reducing agent which stabilized the colloid[8]. This dispersion was washed using deionized

water and again centrifuged to remove any adsorbed impurities or unreacted species. The centrifugation prevented agglomeration after the washings were stored at 4^0C.

1.1.4 Characterization of synthesized silver nanoparticles

1.1.4.1 UV-VIS spectroscopy

The Ag-NPs synthesized was diluted by taking 5 ml into 50 ml volumetric flask with water and mixed well. The dilution was characterized using UV-1850 PC Shimadzu (Tokyo, Japan) spectrophotometer with a quartz cuvette of 1 cm path length at a wavelength range of 300–700 nm. A single, strong and broad Surface plasmon resonance (SPR) peak was observed at 421 nm that confirmed the synthesis of Ag-NPs.

1.1.4.2. Fourier transform infrared (FT-IR) spectroscopy

Spectrum of ampicillin antibiotics, purified Ag-NPs and their antibiotic conjugates were done on a FT-IR spectrophotometer (ThermoScientific Instruments, USA), using KBr pellets/aperture plate. To obtain good signal to noise ratio, 32 scans of ampicillin, purified Ag-NPs and its antibiotic conjugates were taken in the range 4000–400 cm^{-1} and the resolution was kept at 4.0 cm^{-1}[14, 15].

1.1.4.3. Dynamic Light Scattering

Zetasizer family Instruments use Dynamic Light Scattering (DLS) technique and also analyze particle mobility and charge (Zeta potential) using the technique of Electrophoretic Light Scattering (ELS), as well as the molecular weight of particles in solution using Static Light Scattering (SLS)[16]. The hydrodynamic size distributions and polydispersity index (PDI) of the silver nanoparticles were analyzed by using dynamic light scattering (DLS) instrumentation [17, 18]. The average particle size, size distribution by intensity as well as PDI by DLS measurements were carried out on a Zetasizer ZSP particle sizing spectrometer at 25°C with a fixed angle of 90° on highly diluted aqueous samples in this range [17, 18].

1.1.4.4 Ampicillin conjugation to Ag-NPs using cyclic voltammetry

The working electrodes were sonicated for 10 minutes in Milli-Q water to make them clean and thereafter polished using a micro cloth pad (Buehler) with 0.3 µm alumina slurry (Electron Microscopy Sciences). All solutions were degassed with nitrogen for 10 minutes prior to measurements taking place.

To determine the maximum ampicillin conjugation with Ag-NPs, an electrochemical technique using cyclic voltammetry (CV) was undertaken by a conventional three-electrode setup and referenced against Ag|AgCl. This reference electrode had a silver wire in saturated solution Ag|AgCl making up a half-cell, separated with a porous glass frit. The electrochemical properties of the nanoparticles were probed using a vitreous carbon working electrode (0.07070 cm^2) which was loaded with Ag-NPs/ antibiotic (2) by drop-casting 5 µL of 1 mM sample and

permitted to dry under ambient conditions. This electrode was also used to measure the electrochemical window of the system without loading. Platinum (Pt) a highly ductile, malleable and unreactive metal which is also resistant to corrosion and stable at high temperatures was applied as the counter electrode. Polycrystalline silver (0.0317 cm^2) macro electrode was used as a working electrode which also was used as a standard to measure the degree of facile Ag nanoparticle oxidation. The method described by [19] using the theoretical value of 400 μC cm^{-2} for full coverage of lead on silver. Ampicillin (2) conjugation to Ag-NPs was done using a cyclic voltammogram (CV), carried out with an initial potential of -600mV/s applied to the working electrode and ramped positively at a sweep rate of 100 mV/s to a predetermined switching potential of -1300mV/s, at which the ramping direction was reversed.

1.1.5. Results and discussion

1.1.5.1. Synthesis and Optimization Studies for Ag-NPs Production

Studies have been done to optimize Ag-NPs properties such as size, shape, etc.to obtain effective ways for their synthesis[16]. Optimization was carried out to improve some Ag-NPs physico-chemical properties. Validated Ag-NPs production methods, though well-developed their optimization was necessary to enhance better product yield. This resulted in shorter reaction times and low-cost nanoparticles with greater antimicrobial activity.

This work shows the possibility of improving Ag-NPs synthesis by using the same method, but making changes in four parameters: silver nitrate concentration, temperature, and pH of the solution. The variables were, i) area under the curve of the UV-VIS absorbance spectrum; ii) the average size of Ag-NPs iii) the greatest intensity peak in the size distribution of Ag-NPs;

iv) the poly-dispersity of Ag-NPs. These dependent variables were quantified with the following techniques.

1.1.5.2 AgNO3 Concentration Effect

The Ag-NPs with different concentrations of silver nitrate solution 0.007 mm (2mls in 50mls) to 0.036 mm (10mls in 50mls) as illustrated in Figure 1. The optimum concentration for silver nitrate was estimated to be 0.022 mm calculated by Beer-Lambert law.

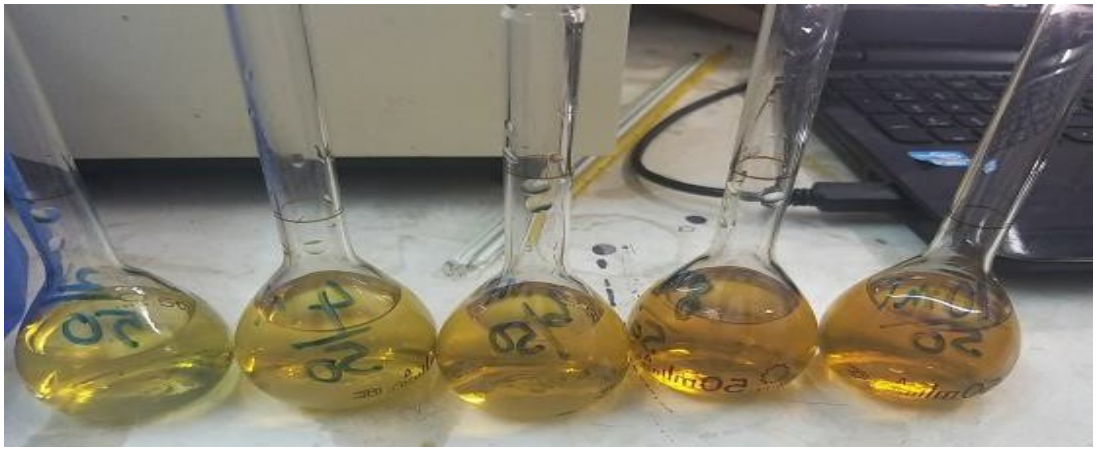

Figure 1: Optimization of AgNO3 Concentration from 0.007 mM to 0.036 mM

In this work, the expected size range was 30-60 nm of the Ag-NPs. The 0.022 mM (5mls in 50mls) silver nitrate concentration gave the expected size range of the Ag-NPs. [8] noted some chemical and other methods for synthesizing and stabilizing Ag-NPs including the use of $AgNO_3$ silver precursor and trisodium citrate as both a reducing and stabilizing agent. This method produced a size range of 30-60 nm of the Ag-NPs.[8]. UV-VIS spectroscopy is quite sensitive to the existence of silver colloids since nanoparticles display a strong absorption peak owing to the surface plasmon excitation. As the concentration was brought to 0.036 mM, the particle size increased because the plasmon absorption shifted red away from 400 nm [19]. The absorption band for typical Ag-NPs ranges in the region of 350 nm to 450 nm[20]. The absorbance Ag-NPs using 0.007 nm to 0.036 nm concentrations gave a spectra maxima peak of 425 nm Figure 2. The higher concentration of the metal precursor and the reducing agent (trisodium citrate), the larger the probability of obtaining Ag-NPs, due to the availability of the substrate and the ability of trisodium citrate to release electrons to the oxidizing agent and reduce the silver in the nanoparticles[21]. This study results correlate with [22] and [23] who used 1.0 mM $AgNO_3$ to produce Ag-NPs using the fungus *Rhizopus stolonifera* [22, 23].

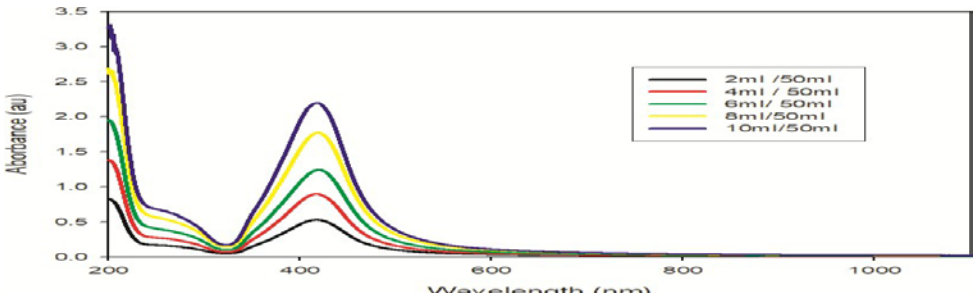

Figure 2: Ag-NPs Absorbance for Concentration/Volume

1.1.5.3 pH Effect

pH values strongly altered the electrical charges of biomolecules and trisodium citrate capping agent thereby changing their binding power and then reducing metal ions [24]. These pH effect was investigated over pH 4-8 values as illustrated in Figure 3. Absorption spectra in these values showed surface plasmon resonance (SPR) peak shifting towards shorter wavelength region. Thus raising pH of the solution, forms smaller sized nanoparticles and vice versa. Similarly, a broadening shows the existence of a wider range of sizes in the solution [25].

The neutral pH 7.0 gave the expected size (30-60 nm) with an absorption peak of about 425 nm, acidic pH (4-5) produced those below 400 nm, and basic medium pH 8 produced those shifted red towards 428 nm. The basic medium (redshift) produced broad Ag-NPs compared to neutral and acidic conditions and [26] interpreted the change in shift according to the presence of large particles that in need have less excitation energy. In support of these current results, [27] reported that at some acidic pH, the nuclei of Ag^{+} ions are created growing to a huge number of nanoparticles with lesser diameters.

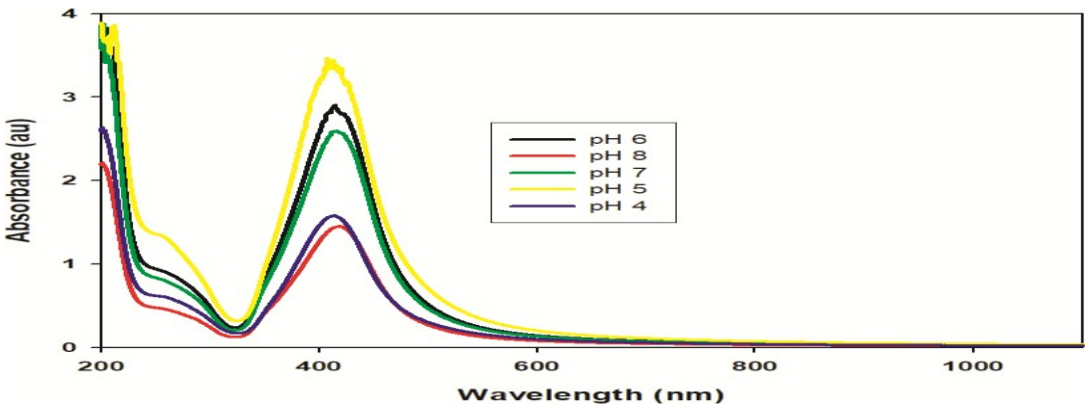

Figure 3: Ag-NPs Absorbance for pH

1.1.5.4. Temperature Effect

The temperature effect on Ag-NPs production was optimized from 50 °C to 80 °C. The maximum production of Ag-NPs was accomplished at 70 °C by a change in colour within 1-2 hours. The 70 °C-experiment, exhibited a fast colour change, with a final bright yellow colour.

To be practical, a method validation needs to be carried out to apply the experiment at 70°C. The UV- VIS characterization indicated that the absorbance increased with higher temperature and shifted slightly to shorter wavelengths. A single SPR became more distinctive with absorption and the thermometers were visible. This indicates that the Ag-NPs aggregate very maxima of about 425 nm which indicated the production of Ag-NPs [28]. On the other side at high temperatures 80°C and above, silver traces on the Erlenmeyer flasks quickly at this temperature range as expressed in Figure 4.

According to Gibbs free energy of formation of spherical crystals, higher temperatures led to more negative Gibbs free energy, which was expected to produce smaller (critical radius) size of the Ag-NPs in solution for a supersaturated solution. However, when the temperature is too high, it could lead to extremely fast aggregation [29]. High temperature leads to high reaction kinetics that hinders controlling the growth stage of the crystallization process, leading to uncontrolled and fast aggregation [30]. This kinetics yields a larger diversity of particle sizes compared to cases with the samples from the 70°C-experiments. This results in a broader SPR peak and a darker colour of the sample.

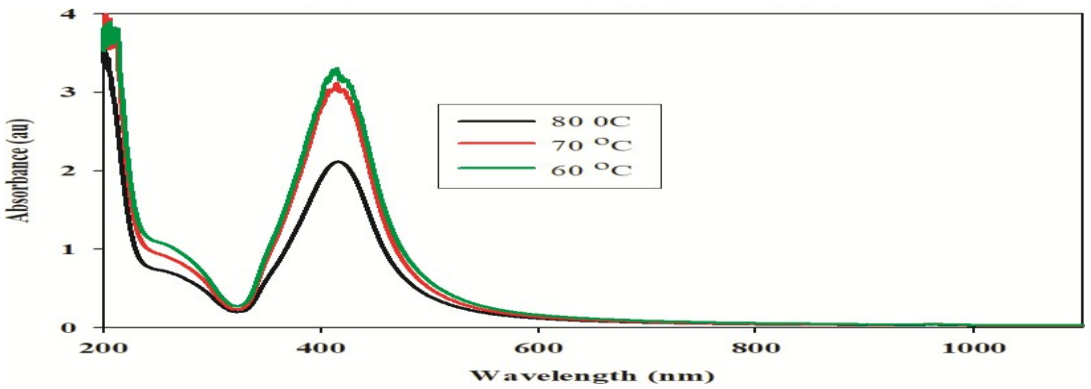

Figure 4: Ag-NPs Absorbance for Temperature

1.1.5.5. AgNO3 Mass Effect

Different masses of silver nitrate (22.5mg, 45mg, 67.5mg, and 90 mg) were used for the chemical synthesis of Ag-NPs[31]. In this work, 90 mg mass for silver nitrate was estimated by a colour change and with UV-visible spectra maxima peak of 410 nm Figure 5. An increase in silver nitrate mass to 90 mg encouraged an apparent increase in the absorbance of the resulted peaks; (0.119, 0.308, 0.521, 0.728, & 0.927). These present results correlate with [8] who used 90 mg $AgNO_3$ to produce Ag-NPs and trisodium citrate as a capping/stabilizing agent.

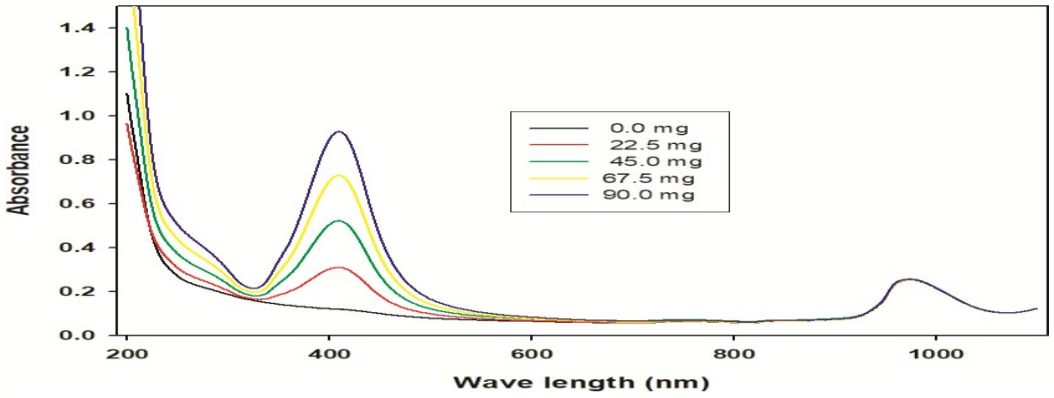

Figure 5: Ag-NPs Absorbance for Mass.

1.1.6. Silver Nanoparticles Synthesis Discussion

The AgNO3 readily dissolved in water and dissociated into its ions giving a redox reaction as per the Equilibrium Law. Forward reaction favored Ag-NPs synthesis, but not the backward one [8]. The dispersion was stored at a temperature of 4°C, under liquid nitrogen to stop this backward reaction, carried out in the dark to protect the Ag-NPs from light as they are susceptible to oxidation. The darkness was achieved by storing the Ag-NPs colloid in a dark (amber) bottle which was then wrapped in an aluminum foil.

Ag^+ is reduced in an aqueous solution, receives an electron from a reducing agent, switches a zero-valent state (Ag^0), then nucleates and grows a process governed by reaction temperature, pH, concentration, precursor type, reducing and stabilizing agents, and a molar ratio of surfactant/stabilizer and precursors[32]. Ag-NPs were synthesized successfully by mixing silver nitrate ($AgNO_3$) as starting raw material and trisodium citrate ($C_6H_5O_7H_3$) as a stabilizing/capping agent producing particles with a nano size range of 41-43 nm. [8] give the particle size of 30-60nm when $AgNO_3$ and $C_6H_5O_7H_3$ were used [8]. This work observed that the injection of the stabilizing solution into a hot solution was an effective avenue of inducing rapid nucleation in the shortest period. Due to the ionic nature of $AgNO_3$, it readily dissolved in water and dissociated into its constituent ions.

$$AgNO_3+2H_2O\rightarrow Ag^+ +NO_3^- +4H^+ +O_2$$

When trisodium citrate was used to reduce the silver salt, the following chemical reactions took place.

$$12AgNO_3+4Na_3C_6H_5O_7+6H_2O\rightarrow 12Ag^+ +12NaNO_3+4C_6H_5O_7H_3+3O_2$$

$$4Ag^+ +Na_3\,C_6H_5O_7+2H_2O\rightarrow 4Ag^\circ +C_6H_*O_7+3Na^+ +H^+ +O_2$$

The $C_6H_5O_7H_3$ averted aggregation of the Ag-NPs by lowering the surface tension between the solid particles and the solvent. This was achieved through adsorption of stabilizer-ions onto the Ag-NPs in solution. The $C_6H_5O_7H_3$ ensured the formation of metal-surfactant complexes in the reaction solution. This reduced the reactivity of the $AgNO_3$ and reduction process rate. As reduction and crystallization occurred concurrently, the nucleation process got favored due to enough gathering of reactants in solution to preserve supersaturation. Moreover, the adsorbed stabilizer-ions created electrostatic repulsion between the coated Ag-NPs, thereby increasing stability. This is essential for narrow size distribution of the particles[10].

A surfactant maybe manipulated to shape during the reduction process (capping). The surfactant prefers binding to certain planes of the crystal system, allowing the "unprotected" planes to be reduced. The stabilizing mechanism is schematically depicted in Figure 6. Besides the reduction of Ag+ ions, citrate ions influence particle growth at early stages by complexing with positively charged Ag^{2+} dimers. Fewer seeds formed in the citrate reduction method and slow cluster growth contribute to the formation of larger silver nanocrystals of varying shape and size.

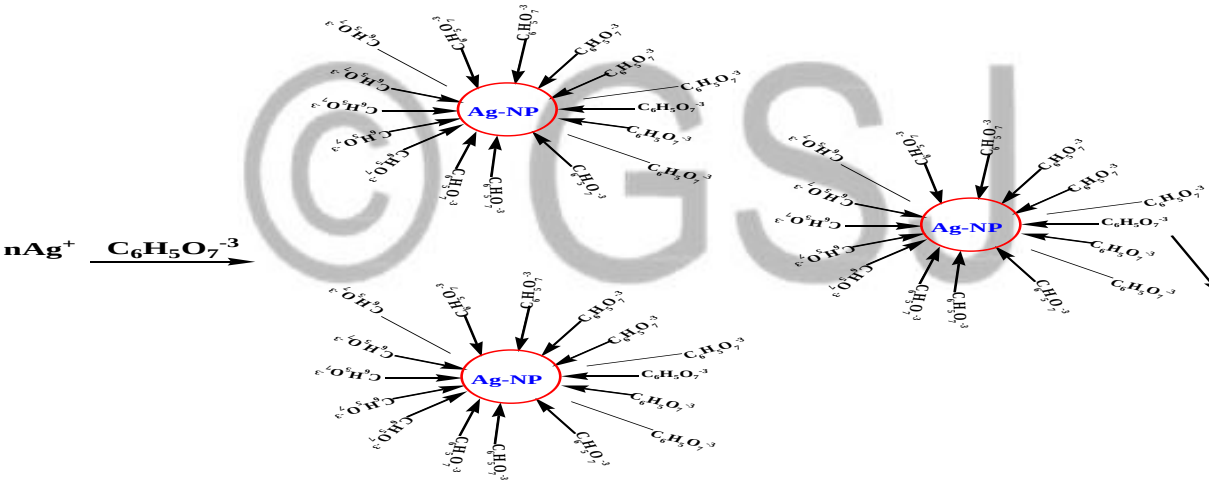

Figure 6: Stabilizing mechanism of trisodium citrate (citrate ions).

Utilizing $C_6H_5O_7H_3$, being a weaker reductant results in a slower reduction rate, has more conducive to controlling the shape and size distribution of NPs[10]. Dropwise addition of a 10 ml aliquot 1 % $C_6H_5O_7H_3$ solution into the boiling $AgNO_3$ solution yielded a dark grey dispersion of Ag-NPs indicating a chemical protocol based on chemical reduction of Ag^+ ions by agent $C_6H_5O_7H_3$. This $C_6H_5O_7H_3$ reduced Ag^+ and enhanced the formation of Ag^0, metallic silver, which agglomerated into oligomeric clusters that formed colloidal particles of metallic silver.

Both crystallization and the reduction processes occurred simultaneously, with crystallization process happening out of two events; nucleation and growth. The homogeneous non-valent form

was insoluble which aggregated slowly into embryos through the reaction process. As more metal atoms got added, the nuclei grew to form primary particles of nano-sized scale. The following reaction occurred in Equation.

$$4Ag^{+}+Na_3C_6H_5O_7+2H_2O\rightarrow 4Ag^{\circ}\ (\text{dark grey})+C_6H_5O_7H_3+3Na^{+}+H^{+}+O_2\uparrow$$

During Ag-NPs synthesis, it was critical stabilizing dispersive NPs[33]. The most common strategy as employed by[10].is the use of stabilizing agents that can be absorbed onto the surface of Ag-NPs, to prevent them from further agglomeration, oxidation and protect their shape[10].Stabilization by capping agents may be attained through electrostatic or steric repulsion[10, 34]. For example, electrostatic stabilization may be achieved through anionic species, such as citrate, halides, carboxylates, or polyoxoanions that adsorb or interact with Ag-NPs to impart a negative charge on the surface of Ag-NPs[10, 34].

1.1.6.1 UV-VIS spectroscopy for Blank and Ag-NPs characterization

Optical properties of Ag-NPs exhibit a blue shift or a redshift depending on the size and shape of nanoparticles[35]. Conduction band and valence band in Ag-NPs lie in very close proximity to one another resulting in free-electron motion[33, 36]. These free-electrons produce a surface plasmon resonance (SPR) absorption band that occurs from the collective oscillation of electrons of Ag-NPs in resonance with the wave light [4, 33]. Redshift (away from 400nm), is for broader larger most scattered peaks, whereas smaller peaks absorb light and have a blue shift near 400nm. As the particles increase in size the plasmon absorption has a redshift and as they reduce in size they shift to blue [33] .

This work obtained a UV-VIS absorption maxima absorbance for Ag-NPs colloid with a blue shift (hypsochromic shift). This indicated narrower distribution since both broadening and a redshift are attributed to an increase in the size of the particles. The smaller in size Ag-NPs peak appears at 421 nm with high absorption values explaining their particles are smaller in size and small width [37]. The 421nm is consistent with the spectra of spherical Ag-NPs within the wavelength range of 350-450 nm confirming formation of nanoparticles with a narrower distribution [38]. The blank produced no peak as also shown in Figures 7 to 9 below. These research results agree with [33, 39] in the Synthesis and Characterization of Silver Nanoparticle by Chemical Route Method.

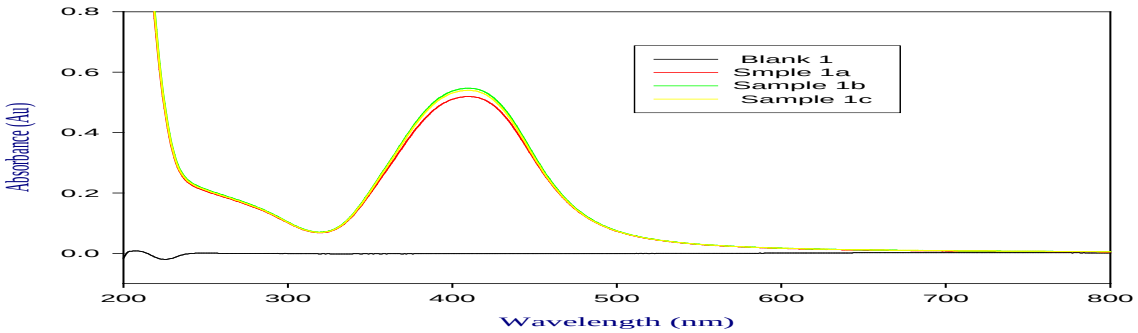

Figure 1: Sample 1 UV-VIS absorption spectrum of Ag-NPs prepared using chemical reduction method

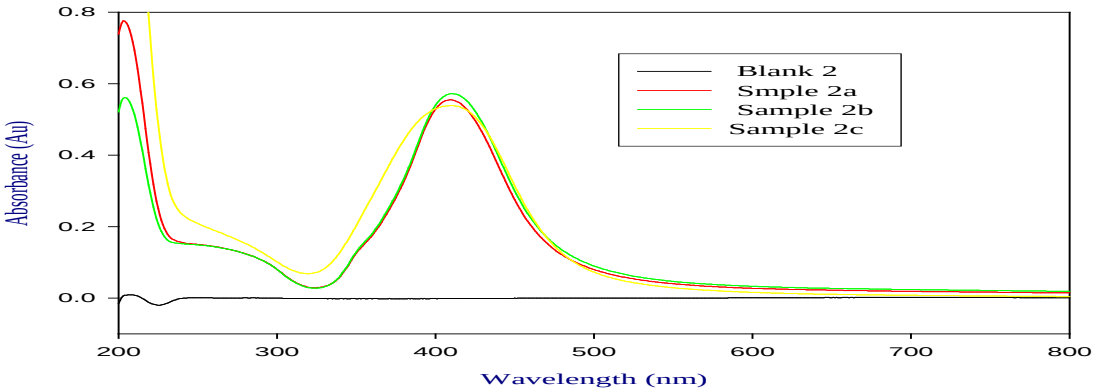

Figure 2: Sample 2 UV-VIS absorption spectrum of Ag-NPs prepared using chemical reduction method

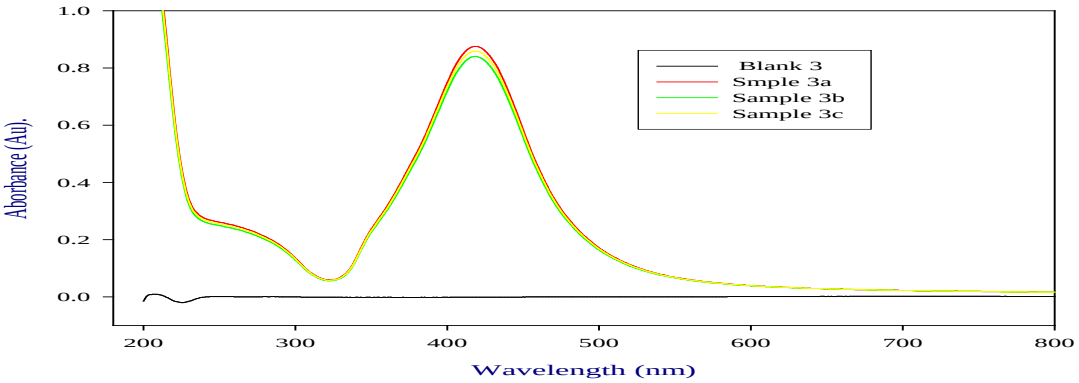

Figure 3: Sample 3 UV-VIS absorption spectrum of Ag-NPs prepared using chemical reduction method

1.1.6.2 FT-IR Spectroscopy Ag-NPs characterization

FT-IR measurements were carried out to identify functional groups within the range of 4000-400cm^{-1} using Shimadzu IRPrestige-21 spectrophotometer.

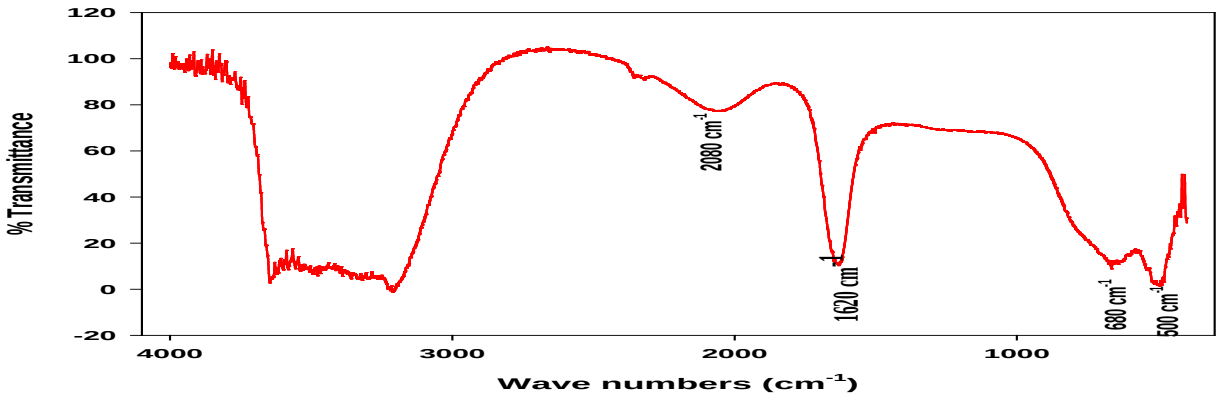

Figure 4: FT-IR spectra of the Ag-NPs chemically prepared by the reduction of silver nitrate with trisodium citrate

The intense bands observed were matched with standard values to ascertain the functional groups. The bands at 3200 cm^{-1} in the spectra correspond to the O–H stretching vibration of carboxylic acid, or alcohol. Due to resonance stabilization, the O-H group gave a broad absorption band in the range 3600 cm^{-1} to 3200 cm^{-1} due to deionized water molecules in the sample. The absorption band at 2080 cm^{-1} ascribes to citrate precursor (-CH_2). The citrated Ag-NPs displayed characteristic vibrations of $C_6H_5O_7H_3$ with a sharp narrow peak at 1620 cm^{-1} to carbonyl stretching (C=O), asymmetrical stretching of citrate.

These functional groups play a role in the stability/capping of Ag-NPs as reported in many studies[40]. The band at 680 cm^{-1} 500 cm^{-1} regions could be attributed (cis) bending or other impurities and the 500 cm^{-1} region could be attributed to C–Br stretching, which is characteristic of alkyl halides and other interfering impurities respectively. This outcome agrees with[41].

1.1.6.3 Dynamic light scattering studies for Particle size distribution, polydispersity and Zeta potential of bare Ag-NPs

The Z-average diameter of nanoparticles was calculated by using the Stokes-Einstein equation[17, 18]. In this work, surface charge of the Ag-NPs was found to influence bactericidal activity, due to their positive charges against the microorganisms tested. The particle size distribution curve illustrated polydispersity, and average diameter of 41-43 nm, zeta potential value of -9.16 to -15.2 mV (Figure 11). The high negative potential value (zeta) backs long term stability, good colloidal nature and high dispersity of Ag-NPs as shown in Table 1 below[42].

Table.1: Size distribution by the intensity of Ag-NPs.

Sample	Z-Average d.nm)	Pdl	Intercept	Zeta Potential (mV)	Zeta Deviation (mV)	Conductivity (mS/cm)
Ag-NPs	42.23	0.556	0.778	-9.16	15.5	0.110

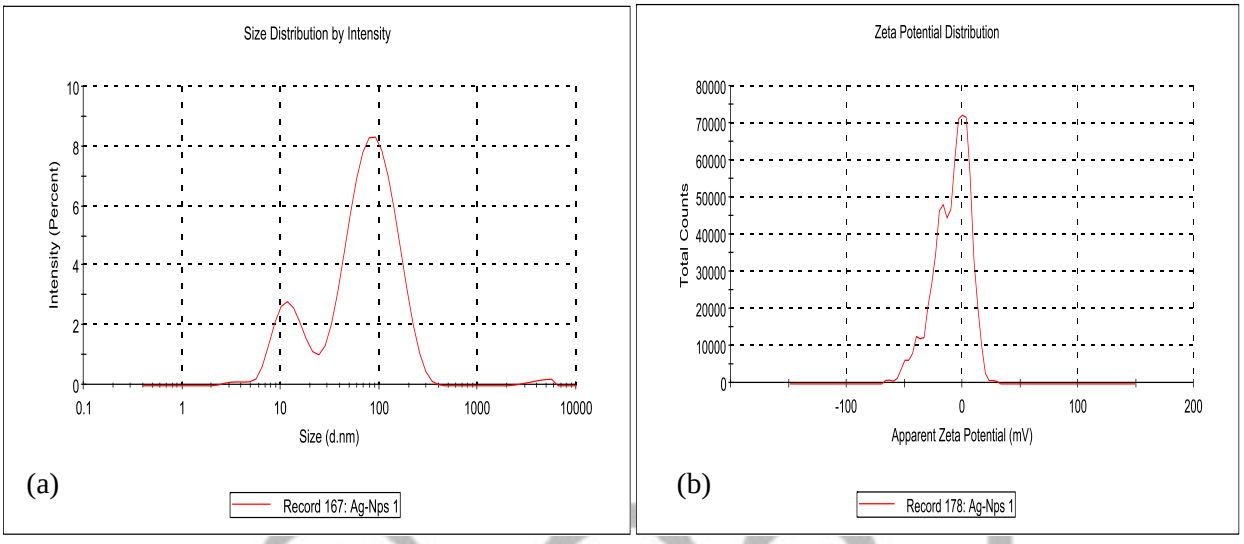

Figure 11: Chart for; (a) size distribution by the intensity and (b) zeta potential distribution of Ag-NPs.

1.1.7 Conjugation Analysis.

Numerous scientific groups have addressed the potential chelation of antibiotics with nanoparticles through the hydroxyl and amide groups, which are present in antibiotic molecules.[6], successfully conjugated Ag-NPs with tetracycline (multiple hydroxyl, phenol, and amide groups. Similarly, functionalized Ag- NPs with glycopeptide antibiotic vancomycin (multiple amides, phenol, and hydroxyl groups). [6] reported successfully the immunosuppressant azathioprine (S-atom and basic N-atoms in heterocycle) with Ag-NPs. Figure 12(a) below illustrates a rectangle encapsulating the free amino group which is the plausible mode of binding of ampicillin (2) with the Ag-NPs and Figure 12(b) its binding route cartoon diagram.

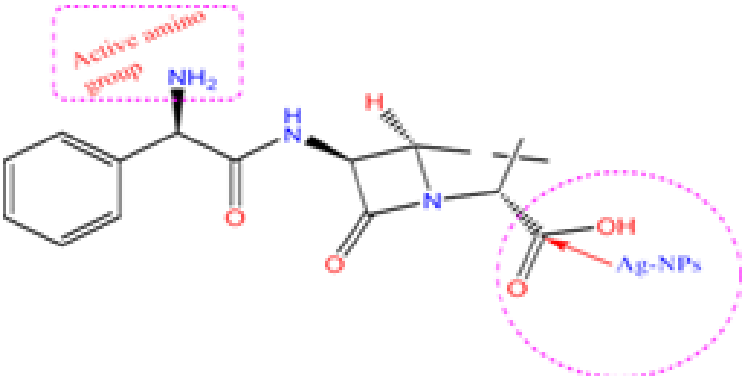

Figure 12 (a): Cartoon illustrating the structure of Ag-NPs bound with ampicillin antibiotic

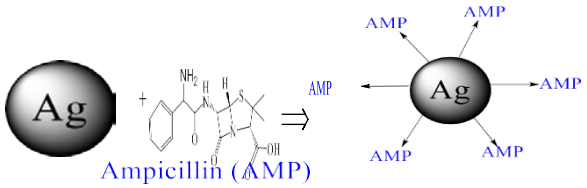

Figure 12 (b): Scheme illustrating the structure of Ag-NPs bound with ampicillin antibiotic

1.1.7.1 UV-VIS studies for synthesized Ag-NPs-2 conjugate

Silver nitrate was reduced with sodium citrate producing Ag-NPs and characterized by UV-VIS spectroscopy. In an aqueous solution, Ag-NPs display a pale yellowish colouration because of the surface plasmon resonance (SPR) of metal nanoparticles. The spectra of UV absorption for Ag-NPs conjugates of antibiotic (2), is illustrated in Figure13.

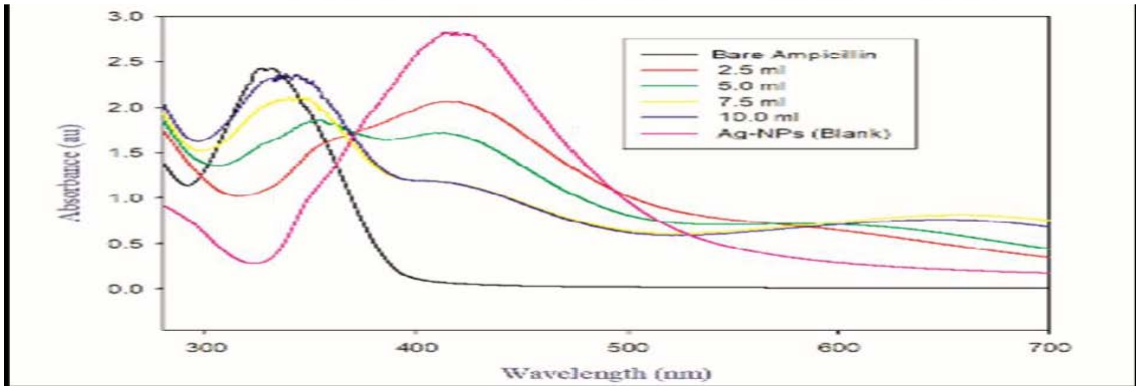

Figure 13 Graph of UV-VIS absorption of Ag-NPs-2 conjugate.

Figure 13, show absorption peaks about at 290 nm, 320 nm, 330nm (UV region), respectively. When antibiotics (2) were conjugated with Ag- NPs solution, the absorption peaks shifted to a shorter wavelength (blue shift) because of charge transfer amongst drug and sodium citrate coated Ag-NPs.

The source of blue shift might be argued on maybe nucleophilic reaction (charge transfer) or

from electronic transitions between different orbital basis. Nucleophilic substitution reaction occurs between lone pair of O atom of trisodium citrate and H atom in the amine group of the antibiotics (2) drugs. Therefore, the sodium citrate acts as a nucleophile in this reaction and boosts electron density, triggering hypsochromic shift for absorption peak. There might be electronic transitions happening amid bonding or non-bonding orbital to antibonding orbital. There can be two main possibilities in electronic transitions: (1) bonding toward antibonding orbital (π-π*) and (2) non-bonding toward antibonding orbital (n- π*). The initial one occurs at low energy (higher wavelength) and the next one requires high energy (lower wavelength). Owing to the existence of lone pair on sodium citrate, the transition from (n -π*) might be extra dominating than (π- π*), which effects the blue shift. Thus, trisodium citrate performs a bridge amid drug and Ag-NPs surface with the blue shift accredited to the drug attachment with Ag-NPs surface. This research outcome concurs with RSC Adv., 2019, 9, 1095 paper.

1.1.7.2 FT-IR studies for synthesized Ag-NPs-2 conjugate.

The FT-IR spectrum of pure (2) showed the bands at 3250 cm^{-1}, 1690 cm^{-1}, 1605 cm^{-1}, 1417 cm^{-1}, 1396 cm^{-1} and 1350 cm^{-1} where 3250 cm^{-1} correlated to -OH, 1690 cm^{-1} is C=O stretching vibrations of four-membered ring lactams, 1605 cm^{-1} primary amine and peak at 1417 cm^{-1}, 1396 cm^{-1} and 1350 cm^{-1} were contributed to characteristic β lactam ring vibrations (Figure 14). For Ag-NPs-(2) in (subsequent part Figure 14), the peak at 1625 cm^{-1} is due to the amine group, which has been shifted to a higher wavenumber when compared to the primary amine of pure (2) (1605 cm^{-1}), this defines the role of the primary amine group of (2) and trisodium citrate in reduction of Ag-NPs-2.

The β-lactam ring bands and other bands do not show any shift in Ag-NPs-2 as compared to pure (2). Hence it can be concluded that while the formation of Ag-NPs-2, β-lactam ring of (2) preserves its integrity. FT-IR data deduces the possibility of H atom of the amines or amides which binds to the O atom in the trisodium citrate which was free for the attachment on the surface of the silver. Figure 16 shows the typical FT-IR spectra of KBr, trisodium citrate, antibiotic (2), Ag-NPs (blank) and Ag-NPs-(2) conjugate superimposed. Penicillin-based drugs contain various amino and hydroxyl groups hence mostly two types of bonding take place between these drugs and Ag-NPs; one is amino bonding (through amine or amide group) and the other is thiol bonding. A similar result has been reported by [14]

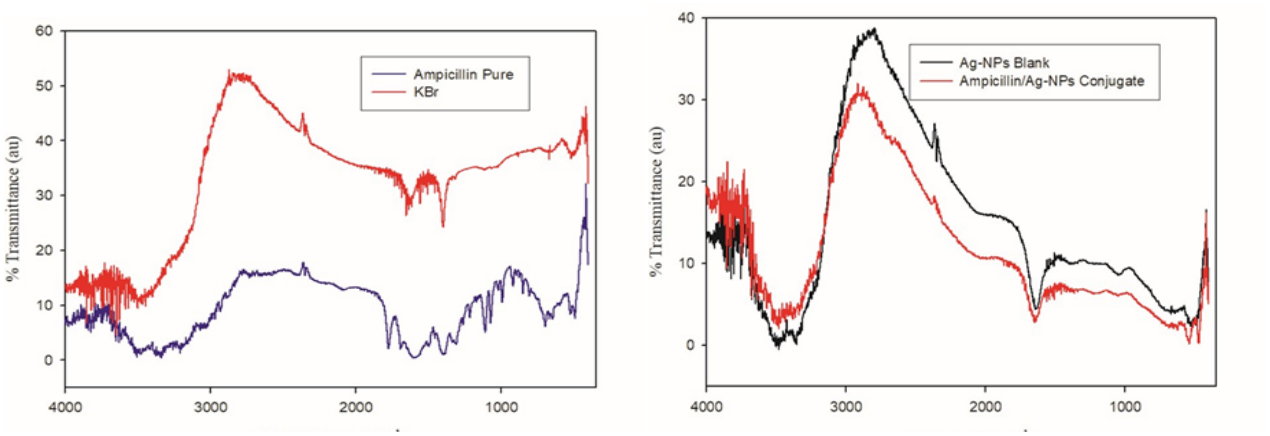

Figure 14: FT-IR spectrums of the pure Ampicillin (2) and Ag-NPs/ Ampicillin (2) conjugate respectively.

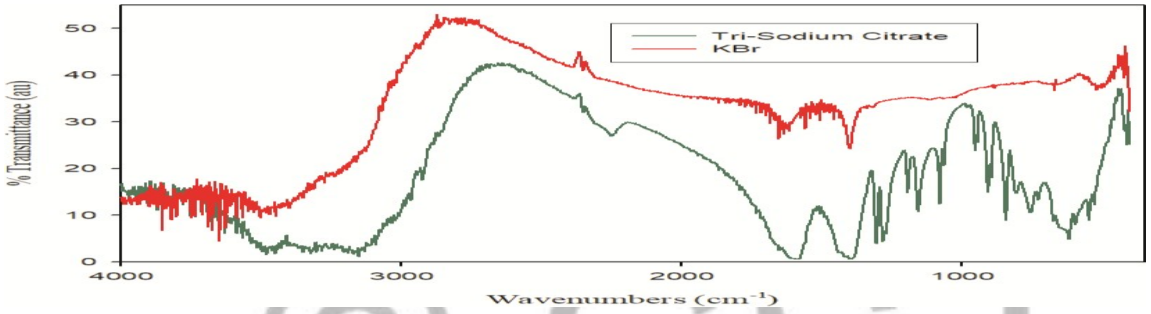

Figure 15: FT-IR spectrum of Tri-Sodium Citrate (Capping Agent).

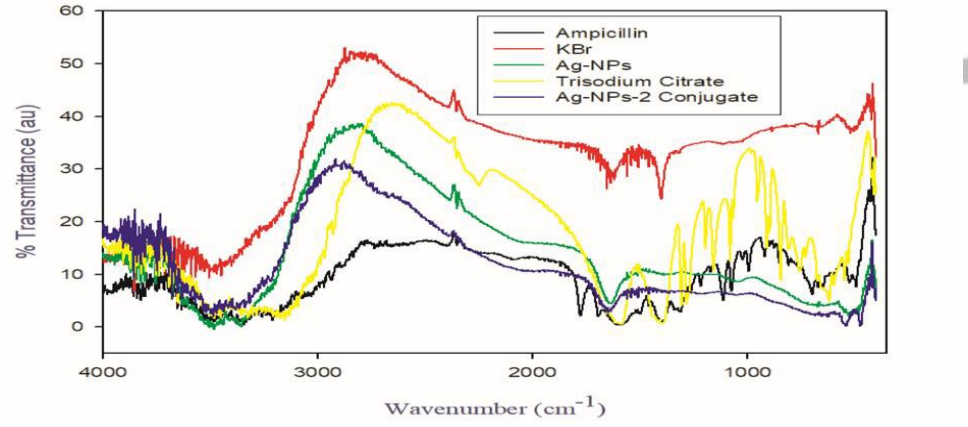

Figure 16: The infrared spectrum comparison of Ampicillin, KBr, Ag-NPs, Ag-NPs-2 Conjugate, and Tri-Sodium citrate.

1.1.7.3.Cyclic voltammetry determination of Ag-NPs conjugates of Ampicillin (2)

For this study, raw materials for Ag-NPs production, pure Ampicillin (2), and Ag-NPs/ Ampicillin (2) conjugate were studied for their CV to gauge whether there was peak enhancement upon conjugation or not and whether the peak shifted towards anodic sides or

cathodic sides. In Figure 17 below, trisodium citrate showed peaks observed in the anodic scan that started at -0.4 mV/s and swept forward to more positive, oxidative potentials.In the anodic scan, three peaks were observed at -0.25V, 0.20V, and 0.50 V; while a single broad peak was observed in the cathodic scan at 1.00 V. Half reactions swiftly exchanged electrons at the working electrode; becoming electrochemically reversible couples. The position of the peaks on the potential axes (*Ep*) is related to the equilibrium potential of the redox process. The equilibrium lies between E_{pa} and E_{pc}, resulting in the difference between the peak potentials for a reversible couple, justified trisodium citrate Nernstian behavior as given in the two Equations below.

$$E^{\circ} = \left(\frac{E_{pa} - E_{pc}}{2}\right) \; and \; E_{pa} - E_{pc} = \left(\frac{0.059\ V}{n}\right)$$

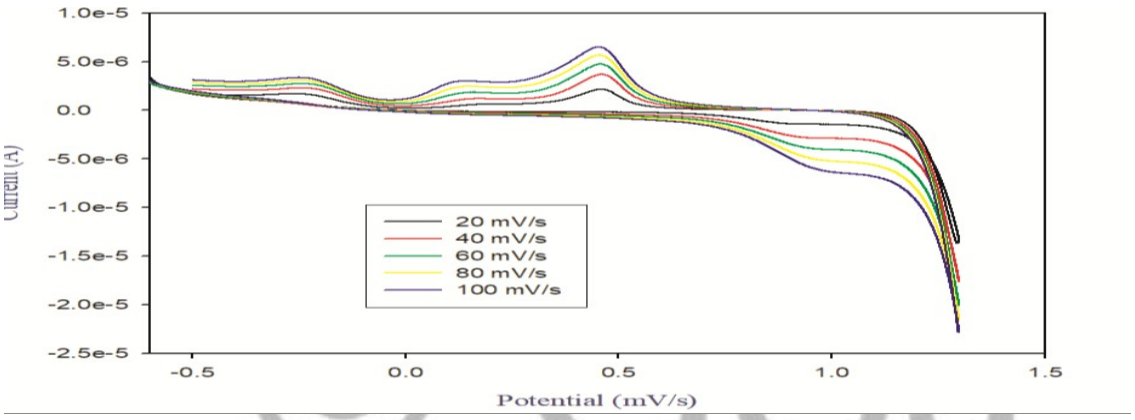

Figure 17: Voltammogram of Trisodium Citrate Oxidation-Reduction

$AgNO_3$ in Figure 18 below, illustrates both oxidative and reductive scans. The current reached peak maximum (anodic peak current (Ipa) for oxidation at the anodic peak potential (Epa), the process undergoes mixed control: more positive potentials increased the current which got offset by $AgNO_3$ decreasing flux further distance from the electrode surface. Reductive scan reduced AgNO3 until the applied oxidized $AgNO_3$ which accumulated the electrode surface was re-reduced. The process has a cathodic peak (Ipc) at the cathodic peak potential (Epc).

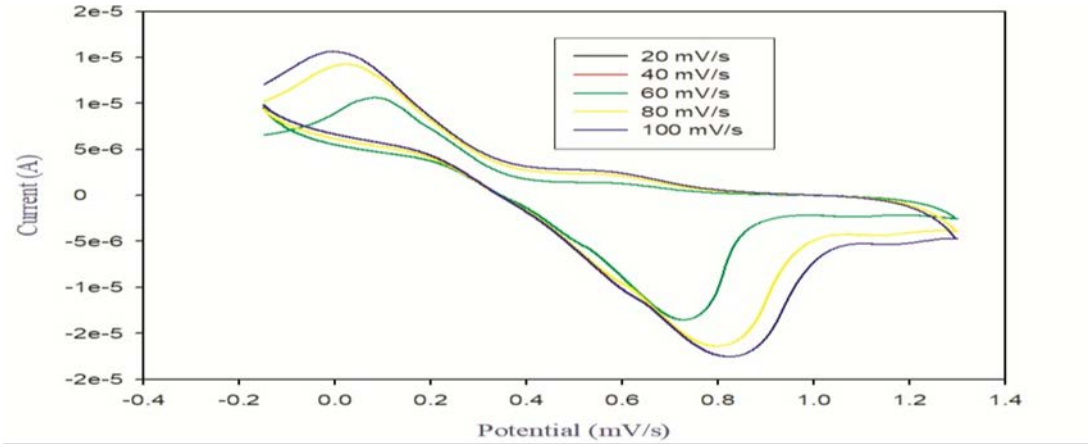

Figure 18: Voltammogram of Silver Nitrate Oxidation-Reduction

In Figure 19, below show pure antibiotic (2) and its conjugate respectively, pure antibiotic (2) give maximum I_{pc} and E_{pa}.Ag-NPs conjugate of (2) gave maximum I_{pc} at about 3.0×10^{-6} A while the E_{pa} shifted towards anodic side at 0.47 mV/s. However, in the case of Ag-NPs conjugate of (2), an extra anodic peak with I_{pc} of 0.5×10^{-6} A and E_{pa} at 0.16 mV/s and cathodic peak with I_{pc} of -2.5×10^{-6} A and E_{pa} at 0.82 mV/s were observed.

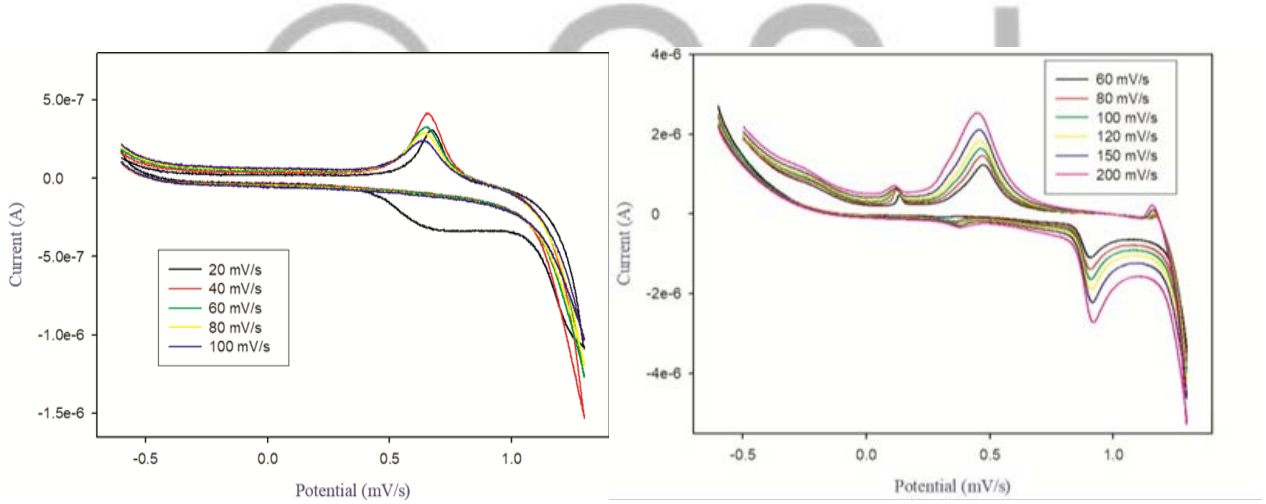

Figure 19: Voltammograms of Ampicillin (2) Oxidation-Reduction and Ampicillin (2) Conjugated with Ag-NPs Oxidation-Reduction

According to Figure 20 and its subsequent (Figure 20), the cyclic voltammograms show the shifting of the anodic and cathodic peak potentials with an increasing trend, which indicates efficient mass transfer between the electrodes' surfaces. CV measurements tell that the ampicillin molecule does not vary the redox properties of the Ag-NPs but they lose their redox properties upon getting bonded with Ag-NPs. This confirms that the ampicillin molecules

get attached on the surface of Ag-NPs. A similar work has been done by [43] in relation to the role of Au(NPs) in the enhanced response of Au(NPs)-decorated Multi-Walled Carbon Nano Tubes (MWCNT) electrochemical biosensor[43]. Figure 20 subsequent shows the typical voltammograms of Ampicillin (2), Ag-NPs-2 Conjugate, trisodium citrate, and Silver Nitrate compared at 80mV scanning potential. CV measurements reveal that the Ampicillin (2), molecule do not vary the redox properties of the Ag-NPs but they lose their redox properties upon getting attached on the surface of Ag-NPs.

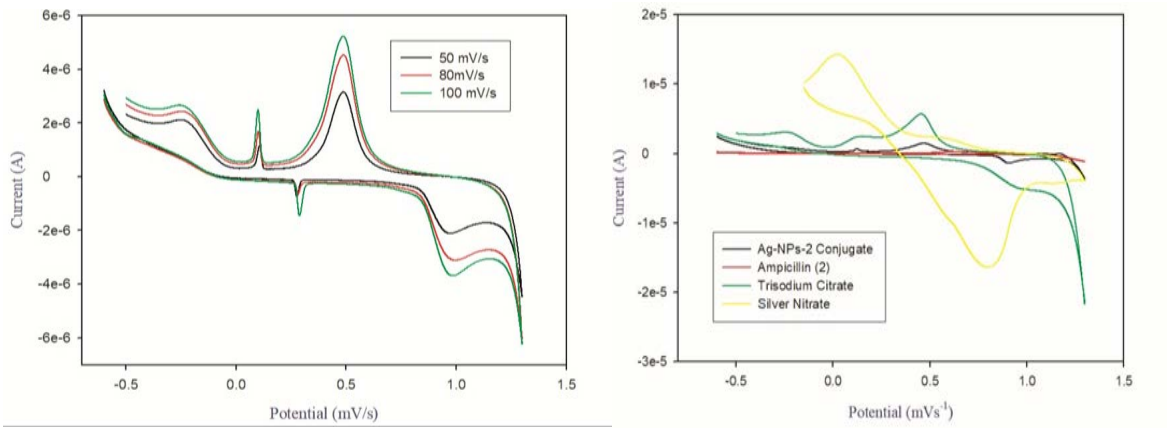

Figure 20: Voltammograms of Ampicillin (2) Conjugated with Ag-NPs Oxidation-Reduction and ampicillin (2), Ag-NPs-2 Conjugate, Trisodium citrate, and Silver Nitrate compared at 80mV scanning potential.

1.1.7.4 DLS Particle size distribution, polydispersity index (PDI) and Zeta potential of Ag- NPs conjugates of ampicillin (2)

The DLS method can be applied to measure narrow particle size distributions, especially between 2–500 nm[44]. Stoke–Einstein equation, concurrently calculated Z-average diameter for Ag-NPs conjugates of antibiotic (2) at around 120.3nm and with PDI of 0.269. Their zeta potentials were obtained as -19.7mv with conductivity of 0.192mS/cm for Ag-NPs/antibiotic (2) conjugate. illustrated in the below table 2.

Stoke–Einstein equation, concurrently calculated Z-average diameter for Ag-NPs conjugates of antibiotic (2) at around 120.3nm and with PDI of 0.269. Their zeta potentials were obtained as -19.7mv with conductivity of 0.192mS/cm for Ag-NPs/antibiotic (2) conjugate. The Z-average size is within the range 2–500 nm described by Russian scientists [44] and therefore, this enhanced Z- average size of Ag-NPs conjugate of (2), hence confirming drug packing on Ag-NPs surface.

Table 2: Average size distribution and Zeta potential of Ag-NPs-2.

Sample	Z-Average (d.nm)	PDI	Intercept	Zeta Potential (mV)	Zeta Deviation (mV)	Conductivity (mS/cm)
Ag-NPs- 2	120.3	0.269	0.905	-19.7	8.42	0.192

1.1.7.5 *In vitro* assay and LD50 of the novel Ag-NPs conjugates of antibiotic (2) against *E. coli* and *S. aureus.*

Two common and available in the laboratory then, bacterial model strains *i.e. S. aureus* (Gram-positive) and *E. coli* (Gram-negative) were used in this investigation. The novel Ag-NPs conjugates of antibiotic (2), showed significant bacterial effects against Gram-negative *E. coli* and Gram-positive *S. aureus*. Silver metal was selected as a carrier for the nanoparticle-based drugs since it is easily available, inert, and biocompatible [45]. According to Antimicrobial Resistance surveillance systems from WHO, (2017) [46], there are 8 bacterial pathogens responsible for human infections, namely: *Shigella spp., Klebsiella pneumoniae, Staphylococcus aureus, Acinetobacter spp., Neisseria gonorrhoeae, Escherichia coli, Streptococcus pneumoniae, and Salmonella spp*. Because of the availability of the standard microorganisms in the laboratory, the study used *E. coli* and *S. aureus*.

Antibacterial efficacy of Ag-NPs with or without conjugation with drugs was expressed in terms of zone of inhibition (ZOI). For each strain, ZOI for pure drugs and Ag-NPs conjugates (2), were calculated by the agar-well diffusion method. Microorganisms grew actively to reduce potentially INT to a purple-red colour, indicating that viable cells turn purple and the dead remain colourless indicating no growth. The positive results obtained bacterial growth in antibiotic (2) but negative for blank. In this work Table 3, show the growth inhibition zone diameters, their mean and standard deviation in millimeters (mm) that were measured.

Table 3: The Zone of Inhibition diameters, mean and standard deviation (mm) of Ag-NPs, antibiotic (2), and Ag-NPs-2.

Analytes	Plates	*E.coli*	*S.aureus*	Mean	SD	Mean	SD
-	-	-	-	*E.coli*	*E.coli*	*S.aureus*	*S.aureus*
Ag-NPs	1	0	0	0	0	0	0
Ag-NPs-2 conjugate	1	11	12	11	0	12	0
Amp	1	8	6	8	0	6	1

Key: Ag-NPs - silver nanoparticles, Ag-NPs-2 - conjugate of silver nanoparticles with ampicillin, AMP-ampicillin.

Table 3 shows the mean zone of inhibition (ZOI) for Ag-NPs being zero in both the *E.coli* and *S. aureus* samples respectively. The zero antibacterial effect against both strains might be due to low concentration. The Ag-NPs-2 conjugate had a mean ZOI of 11 and 12 in *E.coli* and *S aureus* samples respectively. The mean ZOI of ampicillin (2) was 8 and 6 in *E. coli* and *S. aureus* samples respectively.

The Ag-NPs based antibiotic conjugate enlarged the zone of inhibition (ZOI) of antibiotics significantly (Table 3). Ag-NPs conjugate of antibiotic (2), showed a more enhanced bactericidal effect on *E. coli* than *S. aureus*. *E. coli* are Gram-negative bacteria and when they were treated with Ag-NPs conjugates of antibiotic (2) at different concentrations; they inhibited bacterial growth to some extent. Their ZOI increased from 6 to 8 mm and the bacteria became sensitive to Ag-NPs conjugate of antibiotic (2), as revealed in Table.3.

In the event of *S. aureus*, bacterial growth inhibition also enhanced from 5 to 8 mm. The zone of inhibition with Ag-NPs for both test strains increased from 11-13 and 10-12 for *E.coli* and *S. aureus* consecutively as shown in Table.3 and their corresponding images are shown in Figure 21. Reported studies show some antibacterial activity changes of Ag-NPs conjugates after different treatments. [47], established that the antibacterial activity of Ag-NPs conjugates decreased at low temperatures, as well as after being exposed to low pH. The synergistic effect is due to the efficient delivery of drugs attached to Ag-NPs to bacterial cell membrane which is hydrophobic. Also, antibiotic (2) is hydrophilic while Ag-NPs are hydrophobic.

According to [48] a synergistic antimicrobial effect was observed when combining Ag-NPs and kanamycin according to the fractional inhibitory concentration index, FICI: <0.5), an additive effect by combining Ag-NPs and chloramphenicol (FICI: 0.5 to 1).[49] opined that nanoparticles (NPs) are increasingly being used to target bacteria as an alternative to antibiotics. The antibacterial mechanisms of Ag-NPs are poorly understood, but their currently accepted mechanisms include oxidative stress induction, metal ion release, and non-oxidative mechanisms.

According to [51] and[52] the interaction of NPs with bacterial cell walls accompanied by the release of toxic Ag^{+} ions significantly contributed to the antibacterial action of various Ag-NPs on different Gram-negative and Gram-positive bacteria. In addition, it was also observed that some medically important pathogenic bacteria were inherently more susceptible to Ag-NPs than others.

Reviews by [51], [52], and [53] summarized four main tentative mechanisms of antibacterial action of metal oxide NP: 1) generation of ROS, 2) partial dissolution accompanied by the release of toxic metal ions, 3) NP accumulation on the membrane surface, and 4) cellular uptake of NPs. To reach the plasma membrane (PM) of Gram-negative bacteria, Ag ion/Ag-

NPs should first pass the outer membrane. Most likely, Ag^+ ions pass the outer membrane through porins [52], inducing several toxic events hampering the vital functions of PM. For instance, [54] showed that Ag^+ ions induced dissipation of pH gradient on the membrane of inside-out membrane vesicles of *Vibrio cholerae*. It has also been reported that in comparison to bare Ag-NPs, the drug–Ag-NPs conjugates boost the release of Ag^+ ion which creates a synergetic effect [55].

Table 4: ANOVA analysis for *E. coli*

Source	Sum of squares (SS)	Degrees of freedom (νν)	Mean square (MS)	F statistic	p-value
Treatment	378.5714	6	63.0952	189.2857	$1.3989e^{-12}$
Error	4.6667	14	0.3333	-	-
Total	383.2381	20	-	-	-

As shown in Table 4, there was a significant difference ($p<0.01$) when comparing sample Ag-NPs with samples AgNPs-2, Ampicillin (2). There was a significant difference ($p<0.01$) when comparing sample AgNPs-2 with sample Ampicillin (2). The p-value corresponding to the F-statistic of the ANOVA is lower than 0.05, suggesting that one or more treatments are significantly different.

Table 5: Tukey HSD results for *E.coli* test

	Ag-NPs	AgNPs-2	Ampicillin
Ag-NPs	0	** p<0.01	** p<0.01
AgNPs-2	** p<0.01	0	** p<0.01
Amp	** p<0.01	** p<0.01	0

Key: Ag-NPs - silver nanoparticles, AgNPs-2 - conjugate of silver nanoparticles with ampicillin, Amp-ampicillin, * - $p<0.05$ and ** - $p<0.01$

The p-value corresponding to the F-statistic of one-way ANOVA is lower than 0.05, suggesting that the one or more treatments are significantly different as shown in Table 5.

Table 6: ANOVA analysis for *S. aureus*

Source	Sum of squares SS	Degrees of freedom νν	Mean square (MS)	F statistic	p-value
Treatment	335.1429	6	55.8571	97.7500	$1.2933e^{-10}$
Error	8.0000	14	0.5714	-	-
Total	343.1429	20	-	-	-

Table 6 above, shows there was a significant difference ($p<0.01$) when comparing sample Ag-NPs with AgNPs-2 and ampicillin. There was a significant difference ($p<0.01$) among sample conjugate of AgNPs-2 compared to ampicillin. The p-value corresponding to the F-statistic of the ANOVA is lower than 0.05, suggesting that one or more treatments are significantly different.

Table 7: TUKEYS HSD results for *S. aureus* test

	Ag-NPs	AgNPs-2	Amp
Ag-NPs	0	** p<0.01	** p<0.01
AgNPs-2	** p<0.01	0	** p<0.01
Amp	** p<0.01	** p<0.01	0

Key: Ag-NPs - silver nanoparticles, AgNPs-2 - conjugate of silver nanoparticles with ampicillin, Amp-ampicillin. * - $p<0.05$ and ** - $p<0.01$.

The LD_{50} decreases with an increase in the concentration of Ag-NPs from 0 ppm to 30 ppm, which shows the improvement of the cytotoxicity of the antibiotics with an increase in the concentration of the Ag-NPs, as shown in Table 8 below.

Table 8: Concentration of Ag-NPs and antibiotic conjugates used in cytotoxicity determination.

Concentration	Ampicillin (2)
Antibiotic (2) + 0 ppm Ag-NPs	400 ppm
Antibiotic (2) + 15 ppm Ag-NPs	300 ppm
Antibiotic (2) + 30 ppm Ag-NPs	200 ppm

The absorbance at 570 nm is highest for a culture without any concentration of antibiotic. The standard used was 50 ppm of antibiotic, and samples of 100 ppm, 200 ppm, and 500 ppm the higher the concentration of antibiotic conjugates, the lower the absorption, Figure 21.

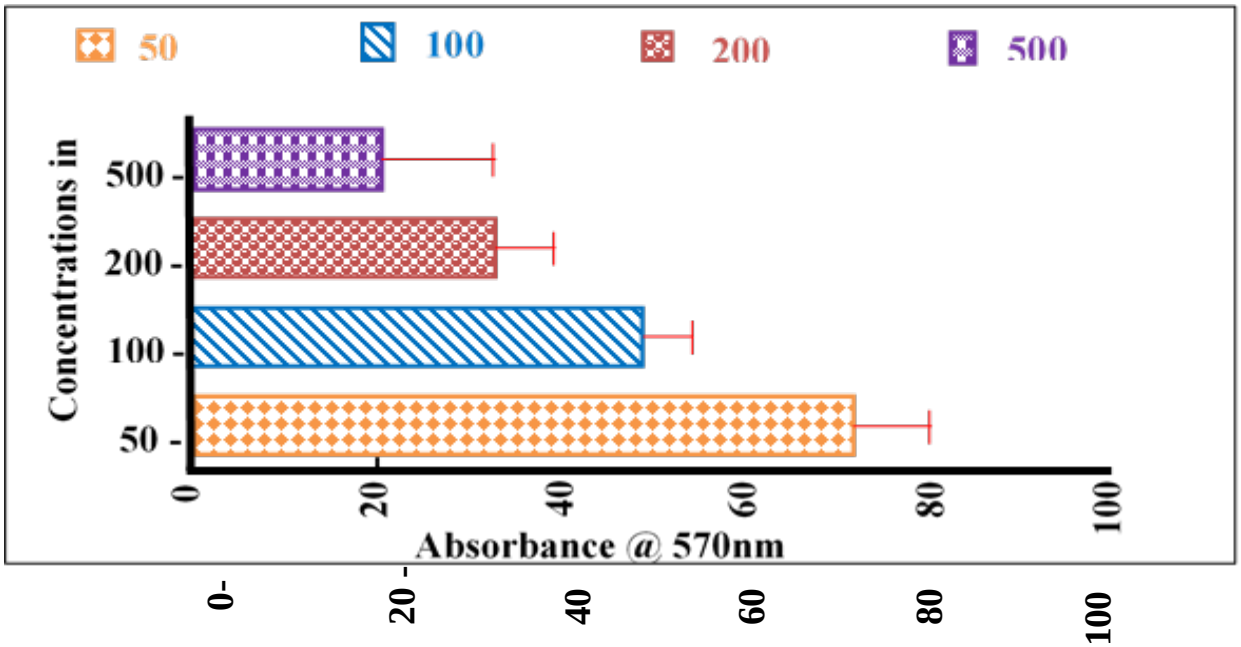

Figure 21: LD50 absorbance@ 570nm vs. concentration in ppm

4.0 Conclusion

The functionalizing of antibiotics with Ag-NPs improved their conductivity, through redox species adsorbing on the electrode surface, which confirmed their conjugation on the surface of the Ag-NPs electrode. Further confirmation studies on the surface chemistry of the prepared Ag-NPs functionalized were studied using UV-VIS spectroscopy where absorption peaks shifted blue, maybe due to nucleophilic reaction or from electronic transitions between different orbitals basis. The Infra-red spectroscopy, illustrated some newer functional groups forming and others vanishing in the conjugates.

Conjugated Ag-NPs showed higher antimicrobial activity to Ag-NPs against *E. coli* and *S. aureus.* Ag-NPs conjugates of antibiotic (2) had average LD50 that is lower than bare antibiotics therefore significantly effective.

5.0 Acknowledgments

The Authors thank TUK University, Chemical and materials department, Multimedia University (MMU) and the Government Chemist, Kenya (GC) for the support that enabled part of the work to be conducted in their respective Institutions. We also wish to thank Mr, Daniel, Mr Samson, Mr Thomas and Dr Magu (MMU), Dr. Gikonyo (MOH,Kenya), Dr Owuor, Dr. Otieno of TUK and Dr Gathirwa for their professional and technical support rendered during the time of the study. Lastly, we thank the management of the KEMRI, Kenya. Finally, we thank everyone that supported the process

REFERENCES

1. Bax, R.G., David., *Introduction to Antibiotic Resistance.* In Handbook of experimental pharmacology 2012: p. 1-12.
2. Pingarrón, J.M., Labuda, Ján, Barek, Jiří, Brett, Christopher M. A., Camões, Maria Filomena, Fojta, Miroslav and Hibbert, D. Brynn., *Terminology of electrochemical methods of analysis (IUPAC Recommendations 2019).* Pure and Applied Chemistry,92(4), , 2020: p. 641-694.
3. Gentile, A., Ruffino, F., & Grimaldi, M., *Complex-Morphology Metal-Based Nanostructures: Fabrication, Characterization, and Applications.* . Nanomaterials, 6(6),, 2016: p. 110.
4. 10. Das, R.N., S.S. & Chakdar, Dipankar & Gope, Gautam & Bhattacharjee, R., *Preparation of silver nanoparticles and their characterization.* J. Nanotechnol, 5, , 2009: p. 1-6.
5. Javed, R., Zia, M., Naz, S. et al., *Role of capping agents in the application of nanoparticles in biomedicine and environmental remediation: recent trends and future prospects.* . J Nanobiotechnol, 18, , 2020: p. 172.
6. Hussain, M.H., Abu Bakar, N.F., Mustapa, A.N. et al., *Synthesis of Various Size Gold Nanoparticles by Chemical Reduction Method with Different Solvent Polarity.* Nanoscale Res Lett, 15,, 2020: p. 140.
7. Sadrolhosseini, A.M., Mohd Adzir & Alizadeh, Farideh & Abdul Rashid, Suraya., *Laser Ablation Technique for Synthesis of Metal Nanoparticle in Liquid.* 2018.
8. Iravani, S., Korbekandi, H., Mirmohammadi, S. V., & Zolfaghari, B., *Synthesis of silver nanoparticles: chemical, physical and biological methods.* . Research in pharmaceutical sciences, 9(6), , 2014: p. 385–406.
9. Łukowiec, D., Radoń, A., *Self-organization of silver nanoparticles during synthesis of Ag–Au nanoalloy by UV irradiation method.* . 2020: p. 2796–2801.
10. Lee, S.H., & Jun, B. H., *Silver Nanoparticles: Synthesis and Application for Nanomedicine.* . International journal of molecular sciences, 20(4), , 2019: p. 865.
11. Heuer-Jungemann, A., Feliu, N., Bakaimi, I., Hamaly, M., Alkilany, A., Chakraborty, I., Masood, A., Casula, M. F., Kostopoulou, A., Oh, E., Susumu, K., Stewart, M. H., Medintz, I. L., Stratakis, E., Parak, W. J., & Kanaras, A. G., *The Role of Ligands in the Chemical Synthesis and Applications of Inorganic Nanoparticles.* . Chemical reviews, 119(8), 2019: p. 4819–4880.
12. Brown, A.N., et al., *Nanoparticles functionalized with ampicillin destroy multiple-antibiotic-resistant isolates of Pseudomonas aeruginosa and Enterobacter aerogenes and methicillin-resistant Staphylococcus aureus.* Applied and environmental microbiology,, 2012. **78(8), 2768–2774.**
13. Rogowska, A., et al., *Silver nanoparticles functionalized with ampicillin.* Electrophoresis, 2017. **38(21), 2757–2764.**
14. 27. Khatoon, N., Alam, H., Khan, A. et al., *Ampicillin Silver Nanoformulations against Multidrug resistant bacteria.* . Sci Rep, 9,, 2019: p. 6848.
15. El-Kahky, D., Attia, M., Easa, S. M., Awad, N. M., & Helmy, E. A., *Interactive Effects of Biosynthesized Nanocomposites and Their Antimicrobial and Cytotoxic Potentials.* Nanomaterials (Basel, Switzerland), 2021: p. 903.
16. Lotfy Walid A., A.B.M., Sabry Soraya A., Ghozlan Hanan A., *Biosynthesis of Silver Nanoparticles by Aspergillus terreus: Characterization, Optimization, and Biological Activities.* . Frontiers in Bioengineering and Biotechnology, 9, , 2021: p. 265.
17. Clayton, K.N., Salameh, J. W., Wereley, S. T., & Kinzer-Ursem, T. L., *Physical characterization of nanoparticle size and surface modification using particle scattering diffusometry.* Biomicrofluidics, 2016.
18. Kaasalainen, M., Aseyev, V., von Haartman, E. et al., *Size, Stability, and Porosity of Mesoporous Nanoparticles Characterized with Light Scattering.* . Nanoscale Res Lett, 12, , 2017: p. 74.
19. Kirowa-Eisner, E., D. Tzur, and E. Gileadi, *Underpotential dissolution of metals under*

conditions of partial mass-transport control. Journal of Electroanalytical Chemistry,, 2008. **621(2), 146-158**.

20. Zomorodian, K. and A. Monfared, *Biosynthesis and Characterization of Silver Nanoparticles by Aspergillus Species.* . BioMed Research International, , 2016. **2016, 1-6.** .
21. Rashid, M.B., Md. Khairul & M. Emran, Quayum., *Synthesis of Silver Nano Particles (Ag-NPs) and their uses for Quantitative Analysis of Vitamin C Tablets.* Dhaka University Journal of Pharmaceutical Sciences, 12., 2013.
22. Brown AN, S.K., Samuels TA, Lu J, Obare SO, Scott ME., *Nanoparticles functionalized with ampicillin destroy multiple-antibiotic-resistant isolates of Pseudomonas aeruginosa and Enterobacter aerogenes and methicillin-resistant Staphylococcus aureus.* Appl Environ Microbiol, 2012: p. 2768-2774.
23. Farjadian, F., Akbarizadeh, A. R., & Tayebi, L., *Synthesis of novel reducing agent for formation of metronidazole-capped silver nanoparticle and evaluating antibacterial efficiency in gram-positive and gram-negative bacteria.* Heliyon, 2020.
24. Banu, A.R., Vandana & Ranganath, E., *Silver nanoparticle production by Rhizopus stolonifer and its antibacterial activity against extended spectrum Î²- lactamase producing (ESBL) strains of Enterobacteriaceae.* Materials Research Bulletin - MATER RES BULL, 2011: p. 1417-1423.
25. Hamouda, R.A., Hussein, M.H., Abo-elmagd, R.A. et al., *Synthesis and biological characterization of silver nanoparticles derived from the cyanobacterium Oscillatoria limnetica.* . Sci Rep, 9, , 2019.
26. Tanabe, I., Tanaka, Y. Y., Watari, K., Inami, W., Kawata, Y., & Ozaki, Y., *Enhanced Surface Plasmon Resonance Wavelength Shifts by Molecular Electronic Absorption in Far- and Deep-Ultraviolet Regions.* . Scientific reports, 10(1), , 2020: p. 9938.
27. Hamida, R.S., et al., *Lichens A Potential Source for Nanoparticles Fabrication: A Review on Nanoparticles Biosynthesis and Their Prospective Applications.* Journal of Fungi, 2021. **7**(4):
28. Jeevanandam, J., Barhoum, A., Chan, Y. S., Dufresne, A., & Danquah, M. K., *Review on nanoparticles and nanostructured materials: history, sources, toxicity and regulations.* . Beilstein journal of nanotechnology, 9, , 2018: p. 1050–1074.
29. Dattu Singh, V.R., Shivaraj Ninganagouda, Jyothi Hiremath, Ashish Kumar Singh, Jasmine Mathew, *Optimization and Characterization of Silver Nanoparticle by Endophytic Fungi Penicillium sp. Isolated from Curcuma longa (Turmeric) and Application Studies against MDR E. coli and S. aureus.* Bioinorganic Chemistry and Applications, 2014: p. 1-8.
30. Nguyen T. K. Thanh, N.M., and S. Mahiddine., *Mechanisms of Nucleation and Growth of Nanoparticles in Solution.* . Chemical Reviews, 114(15),, 2014: p. 7610-7630.
31. Junius, N. and M. Budayova-Spano, *Optimization of crystallization of biological macromolecules using dialysis combined with temperature control.* Journal of applied crystallography,, 2020. **53(3), 686–698.**
32. A., H.M.G., *Beyond the hype: Big data concepts, methods, and analytics.* International Journal of Information Management, 35(2),, 2015: p. 137-144.
33. Dakal, T.C., Kumar, A., Majumdar, R. S., & Yadav, V., *Mechanistic Basis of Antimicrobial Actions of Silver Nanoparticles.* Frontiers in microbiology, 2016: p. 1831.
34. Zhang XF, L.Z., Shen W, Gurunathan S., *Silver Nanoparticles: Synthesis, Characterization, Properties, Applications, and Therapeutic Approaches.* . Int J Mol Sci., 17(9), , 2016: p. 1534.
35. 46. Phan, H.T., & Haes, A. J., *What Does Nanoparticle Stability Mean?* . The journal of physical chemistry. C, Nanomaterials and interfaces, 123(27), , 2019: p. 16495–16507.
36. 2. Al-Zamel, N., Al-Sabah, S., Luqmani, Y., Adi, L., Chacko, S., Schneider, T. D., & Krasel, C., *A Dual GLP-1/GIP Receptor Agonist Does Not Antagonize Glucagon at Its Receptor but May Act as a Biased Agonist at the GLP-1 Receptor.Int. J. Mol.* International journal of molecular sciences, 2020.
37. Henry, J., Mohanraj, K. & Sivakumar, G., *Influence of Cissus quadrangularis Stabilized*

AgNPs and Its Structural, Optical, Antibacterial Analysis: A Comparative Study. . J Inorg Organomet Polym, 26, 2016: p. 312–319.

38. López-Miranda, J.L., Esparza, R., González-Reyna, M. A., España-Sánchez, B. L., Hernandez-Martinez, A. R., Silva, R., & Estévez, M., *Sargassum Influx on the Mexican Coast: A Source for Synthesizing Silver Nanoparticles with Catalytic and Antibacterial Properties.* Applied Sciences, 10(11), , 2021: p. 4638.
39. Michael Ndikau, et al., *'Green Synthesis and Characterization of Silver Nanoparticles Using Citrullus lanatus Fruit Rind Extract'*,International Journal of Analytical Chemistry., 2017. **1-9**.
40. Khatoon, N.M., Jahirul & Sardar, Meryam., *Biotechnological Applications of Green Synthesized Silver Nanoparticles.* . Journal of Nanosciences: Current Research., 2017.
41. Niraimathi, K.L., Sudha, V., Lavanya, R., & Brindha, P., *Biosynthesis of silver nanoparticles using Alternanthera sessilis (Linn.) extract and their antimicrobial, antioxidant activities.* Colloids and surfaces. B, Biointerfaces, 102,, 2013: p. 288–291.
42. Lim, J., Yeap, S. P., Che, H. X., & Low, S. C., *Characterization of magnetic nanoparticle by dynamic light scattering.* Nanoscale research letters, 8(1), , 2013: p. 381.
43. 12. Elamawi, R.M., Al-Harbi, R.E. & Hendi, A.A., *Biosynthesis and characterization of silver nanoparticles using Trichoderma longibrachiatum and their effect on phytopathogenic fungi.* Egypt J Biol Pest Control, 2018: p. 1-28.
44. Mehmood S, C.R., Carlino E, Bhatti AS., 2018 *Role of Au(NPs) in the enhanced response of Au(NPs)-decorated MWCNT electrochemical biosensor.* Int J Nanomedicine, 13, ,: p. 2093-
45. Tomaszewska, E., et al., *Detection limits of DLS and UV-vis spectroscopy in characterization of polydisperse nanoparticles colloids.* . J. Nanomater, 313081., 2013.
46. Wieszczycka, K. and K. Jurga, *Surface functionalization – The way for advanced applications of smart materials.* . Coordination Chemistry Reviews, , 2021. **436, 213846.** .
47. WHO and W. H., *Global antimicrobial resistance surveillance system (GLASS) report: early implementation.* Geneva: World Organization, 2017.
48. Murei, A., et al., Functionalization and antimicrobial evaluation of ampicillin, penicillin and vancomycin with Pyrenacantha grandiflora Baill and silver nanoparticles. Scientific Reports, 2020. **10**(1): p. 11596.
49. Vazquez-Muñoz, R. and A. Huerta-Saquero, *Enhancement of antibiotics antimicrobial activity* due to the silver nanoparticles impact on the cell membrane. . PloS one, , 2019. **14(11),** .
50. Wang, L., Hu, C., and L. Shao, *The antimicrobial activity of nanoparticles: present situation and prospects for the future.* International journal of nanomedicine, , 2017. **12, 1227–1249.** .
51. Mukherjee, S.P., Bondarenko, O., Kohonen, P. et al., *Macrophage sensing of single- walled carbon nanotubes via Toll-like receptors.* . Sci Rep, 8, , 2018: p. 1115.
52. Pavel, D., et al., *Chemiosmotic Mechanism of Antimicrobial Activity of Ag⁺ in Vibrio cholerae*. Antimicrobial Agents and Chemotherapy, 2002. **46**(8): p. 2668-
53. Djurišić, A.B. and Y.H. Leung, *'Toxicity of metal oxide nanoparticles: mechanisms, characterization, and avoiding experimental artefacts.'*. 2015.
54. Mukherjee, S.P., et al., *Macrophage sensing of single-walled carbon nanotubes via Toll-like receptors.* Scientific Reports, 2018. **8**(1): p. 1115.
55. Bhattacharya, P.D., A. , *'An insight into the Mechanism of Antibacterial activity by Magnesium oxide nanoparticles.'*. Journal of Materials Chemistry B., , 2021. **pp. 9.**
56. Liu, Y. and E. Breukink, *The Membrane Steps of Bacterial Cell Wall Synthesis as Antibiotic Targets.* Antibiotics, 2016. **5**(3).